RSC Advances

PAPER

View Article Online
View Journal | View Issue

Cite this: *RSC Adv.*, 2022, **12**, 14838

High-quality all-inorganic $CsPbBr_3$ single crystals prepared by a facile one-step solution growth method†

Mingming Chen, [ab] Youwen Yuan,[b] Yuan Liu, [b] Dawei Cao [*b] and Chunxiang Xu [*a]

Received 24th March 2022
Accepted 6th May 2022

DOI: 10.1039/d2ra01900k

rsc.li/rsc-advances

In this report, a facile one-step solution growth method has been proposed to synthesize high-quality all-inorganic $CsPbBr_3$ single crystals. High-resolution X-ray diffraction, photoluminescence (PL), and current–voltage techniques have been performed to study the properties of $CsPbBr_3$ single crystals. The results have shown that the as-grown $CsPbBr_3$ single crystals exhibited a narrow X-ray rocking curve with a FWHM (full width at half maximum) of 0.043°, a narrow room-temperature PL spectrum with the FWHM of 18.9 nm, and extremely low density of traps (~5.1×10^9 cm^{-3}). The results shown in this work will provide a valuable strategy for the fabrication of high-quality all-inorganic $CsPbBr_3$ single crystals.

Introduction

As emerging materials, lead halide perovskites (LHPs) (ABX_3, A = Cs, CH_3NH_3 (MA), $HC(NH_2)_2$ (FA), *etc.*; B = Pb; X = Cl, Br, and I) have attracted tremendous attention in recent years because of their great success in the field of photovoltaic and photodetection technologies due to their remarkable properties such as long charge carrier diffusion length, high absorption coefficient, defects tolerance and low-temperature solution-processed ability.[1–6] For example, the power conversion efficiency of solution-processed planar perovskite solar cells has reached up to ~25.7% very recently,[7] which is comparable to commercial silicon-based solar cells. Besides, LHPs have also been recognized as promising candidates for light emission applications owing to their competitive optical properties including efficient photoluminescence (PL), narrow-band emission, weak Auger recombination, high optical gain, and widely tunable energy bandgap.[8–16]

Single crystals featured with improved crystalline quality and low density of defects are of vital importance in the development of high-performance optoelectronic devices. LHP single crystals can be grown *via* a low-temperature solution growth process.[17–23] In general, the LHPs nucleate and grow inside the precursor solution containing raw materials (AX and BX_2) and polar aprotic solvents (such as γ-butyrolactone (GBL), dimethyl sulfoxide (DMSO), and *N*,*N*-dimethylformamide (DMF)). In one typical growth process, the supersaturation of precursor solution is achieved through the slow vapor saturation of an anti-solvent (VSA).[18] In such a case, the nucleation and subsequent crystal growth can occur at room temperature (RT), but it produces several millimeter-sized single crystals and further limits the crystalline quality improvements due to the slow species transportation and diffusion at the solid/liquid interface under such a low temperature. In another growth process, the growth of organic–inorganic hybrid LHP single crystals has been reported through invariably heating the precursor solution (HPS). In this case, the supersaturation is realized by slow evaporation of solvent under a constant temperature heating process. Similar to the VSA method, the HPS method produces multiple small-sized single crystals. With the assistance of crystal seeding, millimeter-scale LHP single crystals have been obtained, but a high density of defects have been found at the seed boundaries.[18] Recently, an improved method called inverse temperature crystallization has been proposed by Bakr *et al.*,[19,22] in which the LHP single crystals can rapidly nucleate and grow. However, this method strongly depends on the retrograde solubility behaviors of LHPs, which may limit the variety and quality of as-grown LHPs owing to the limited aprotic solvents available.

Among the typical growth processes mentioned above, the HPS method is simple, low-cost, and convenient, but it has difficulties in growing high-quality large-sized LHP single crystals. In this work, a modified and facile one-step solution growth method has been demonstrated to prepare high-quality centimeter-scale all-inorganic $CsPbBr_3$ single crystals, where the supersaturation of precursor solution was realized *via* a combination of the HPS method and oil bath heating. Specifically, the as-grown $CsPbBr_3$ single crystals exhibited

[a]*State Key Laboratory of Bioelectronics, School of Biological Science and Medical Engineering, Southeast University, Nanjing, Jiangsu 210096, China. E-mail: xcxseu@seu.edu.cn*

[b]*Department of Physics, School of Physics and Electronic Engineering, Jiangsu University, Zhenjiang, Jiangsu 212013, China. E-mail: dwcao@ujs.edu.cn*

† Electronic supplementary information (ESI) available. See https://doi.org/10.1039/d2ra01900k

a narrow X-ray rocking curve (XRC), narrow PL spectrum, and extremely low density of traps.

Experiments

Materials

Lead bromide ($PbBr_2$, >99.5%), cesium bromide (CsBr, >99.5%), dimethyl sulfoxide (DMSO, anhydrous), dimethylformamide (DMF, anhydrous), and silicone oil were used as received.

Growth of $CsPbBr_3$ single crystals

2.4 mmol $PbBr_2$ and 1.2 mmol CsBr were added into 3 mL anhydrous DMSO to form precursor solution. The precursor solution was firstly stirred at 80 °C, and then filtered and heated at 140 °C in a silicone oil bath (as schematically shown in Fig. 1a) in sequence. When invariably heating the precursor, the $CsPbBr_3$ nucleated and grew due to the evaporation of DMSO solvent. The growth process lasted around 5 days. Then, the as-grown $CsPbBr_3$ single crystals were washed by anhydrous DMF and dried in a vacuum for 2 hours in sequence, and finally stored in a vacuum before they were further characterized. For comparison, reference $CsPbBr_3$ single crystals were prepared by HPS method with a same recipe. All experiments were carried out under ambient conditions.

Characterizations

The structural properties of as-grown $CsPbBr_3$ single crystals were characterized by X-ray diffraction (XRD) with Cu Kα radiation of $\lambda = 1.5406$ Å. The optical properties of as-grown $CsPbBr_3$ single crystals were investigated by homemade micro-PL spectroscopy with the excitation of a continuous-wave 405 nm laser. For the excitation power dependence of PL, the excitation power is tuned by an attenuator. The absorption spectra were collected on a UV-VIS spectrophotometer (Agilent Technologies, Cary-8454). The current–voltage (I–V) of Au/$CsPbBr_3$/Au structured device is recorded by Keithley 2401 source-measure unit, where Au electrodes were deposited by a sputtering method at RT.

Stimulation

The steady-state temperature field distribution of precursor solution (solution 1) in the silica glass beaker which is surrounded by silicone oil (solution 2), was numerically calculated using the COMSOL Multiphysics packages. For simplicity, both solution 1 and solution 2 are defined as water in the simulation process. The inner and outer radius of the beaker are 5.0 and 6.3 mm, respectively, and the solution 1 just fills half of the beaker. The beaker is placed in a silica glass container filled with solution 2. The radius of the container is 50 mm, and the height of solution 2 in the container is as twice as solution 1 in the beaker. The container is placed on a heat source. During the simulations, the module of heat transfer in solids and fluids is adopted, in which the heat flux is added at the interfaces between the system and the external environment. The ambient temperature is set as 293.15 K (20 °C), and the temperature of heat source keeps 413.15 K (140 °C). The material parameters for solution 1, solution 2, and silica glass are imported from the material library of COMSOL.

Results and discussions

As reported, the all-inorganic cesium perovskite materials can exhibit various forms of structures such as $CsPbBr_3$, CsBr-rich Cs_4PbBr_6, and $PbBr_2$-rich $CsPb_2Br_5$ according to the connection manner of $[PbBr_6]^{4-}$ octahedra in the unit cell.[24–26] The molar ratio between raw materials (mCsBr : $n$$PbBr_2$) is important for the final crystallization from DMSO solvent. In general, either Cs_4PbBr_6 or $CsPb_2Br_5$ is formed accompanied with the $CsPbBr_3$ under a slight deviation from a perfect ratio of $m : n = 1 : 1$ CsBr : $PbBr_2$.[18,21] To obtain the pure phase $CsPbBr_3$, it is necessary to add additional $PbBr_2$ in the precursor solution since the solubilities of $PbBr_2$ and CsBr in DMSO solvent are quite different (in fact, CsBr is less soluble than $PbBr_2$ in the DMSO solvent). Herein, the precursor solution was prepared by dissolving CsBr and $PbBr_2$ with a molar ratio of 1 : 2 in the DMSO solvent. Notably, only one $CsPbBr_3$ single crystal can be found in the precursor solution during the whole growth process (Fig. 1b). The resulted $CsPbBr_3$ single crystal is cuboid in shape with a size of ~7 mm (Fig. 1c). We anticipate that the

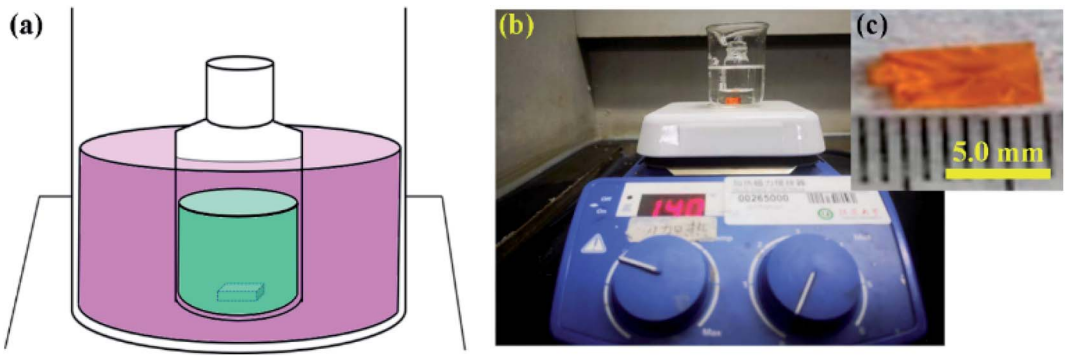

Fig. 1 Growth of $CsPbBr_3$ single crystal. (a) Schematic illustration of experimental setup. Optical images of $CsPbBr_3$ single crystal captured (b) during the growth and (c) at the end of growth.

$CsPbBr_3$ single crystal would grow even bigger when extending the growth time with sufficient raw materials.

XRD measurements were performed to study the structural properties of as-grown $CsPbBr_3$ single crystal. As shown in Fig. 2a and S1 (ESI†), the XRD pattern of as-grown $CsPbBr_3$ single crystal is dominated by the set of (0 0 l)/(h h 0) crystalline plane of orthorhombic $CsPbBr_3$ without traces of Cs_4PbBr_6 and $CsPb_2Br_5$. Generally, $CsPbBr_3$ crystallizes in the orthorhombic space group at RT and it transits to tetragonal and cubic phases at 361 K and 403 K, respectively.[27,28] Interestingly, there is no trace of the tetragonal and cubic phase $CsPbBr_3$ in the as-grown samples. According to the Bragg equation, the lattice constants are calculated to be a = 8.23 Å, b = 8.29 Å, and c = 11.83 Å, which are consistent with the values of $CsPbBr_3$ bulk materials (a_0 = 8.21 Å, b_0 = 8.26 Å, and c_0 = 11.76 Å, obtained from the PDF card: 01-072-7929, Fig. 2b). In contrast, orthorhombic phase $CsPbBr_3$ with slight traces of $CsPb_2Br_5$ were obtained from the HPS method (Fig. S1, ESI†).

The crystalline quality of as-grown $CsPbBr_3$ single crystal was further analyzed by high-resolution XRC measurement, and the result is shown in Fig. 2c. A narrower XRC spectrum suggests a higher crystalline quality. As can be seen, the full width at half maximum (FWHM) of (002) XRC is as small as 0.043° (155 arcsec). This is much smaller than $CsPbBr_3$ single crystal obtained from the HPS method (623 arcsec, Fig. S2, ESI†) and other LHP bulk materials reported in the literature.[18,21,29] Fig. 3a shows the RT PL spectrum of as-grown $CsPbBr_3$ single crystal. As can be seen, the as-grown $CsPbBr_3$ single crystal shows a strong and narrow excitonic emission centered at 532.5 nm (3.328 eV) with the FWHM as narrow as ~18.9 nm (82.5 meV). The narrow PL spectrum can be an indication of the high crystalline quality of as-grown $CsPbBr_3$ single crystal, which is well consistent with XRC results shown in Fig. 2c. In contrast, the PL spectrum of $CsPbBr_3$ single crystals prepared by the HPS method slightly blueshifts (~6 meV) and broadens (~10 meV) (Fig. S3, ESI†), which may be associated with strain induced by the secondary phase (*i.e.*, $CsPb_2Br_5$, shown in Fig. S1, ESI†). In addition, a redshift of the absorption edge is observed (Fig. S4, ESI†), which is caused by the optical absorption in the thick $CsPbBr_3$ single crystal.

Besides, the type of exciton transition from as-grown $CsPbBr_3$ single crystal was then investigated by the excitation power dependence of PL spectroscopy. In general, the relationship between the integrated PL emission intensities (I) and the excitation power (P) follows the eqn (1):[30]

$$I \sim P^k \quad (1)$$

where k is the power coefficient. Qualitatively, for bound excitons and defect-related transitions, the parameter k is less than 1.0, while for free excitons transition the parameter k is higher than 1.0.[30] The PL emission linewidth of as-grown $CsPbBr_3$ single crystal keeps almost unchanged with the increase of excitation power (Fig. 3b inset), suggesting that the excited excitons recombine *via* a similar process. Fig. 3b shows the excitation power dependence of PL emission intensities of the as-grown $CsPbBr_3$ single crystal. The best-fitting gives the power coefficient (k) as 1.45, showing that the RT PL spectra of $CsPbBr_3$ single crystal (Fig. 3b inset) are dominated by the free exciton transition.

Then, the deep-level charged-trap densities in as-grown $CsPbBr_3$ single crystal were further calculated with the space charge limited current (SCLC) theory.[31] Shown in Fig. 4 is the I–V curve of an Au/$CsPbBr_3$/Au structured device. As can be seen, an ohmic region ($I \sim V^n$, $n = 1$) followed by a steep increase ($I \sim V^n$, $n > 3$) can be observed, indicating the presence of a typical trap-filling region. According to SCLC theory, the trap density (n_{trap}) is calculated to be ~5.1 × 10^9 cm^{-3}, from the eqn (2):[31]

$$n_{trap} = 2\varepsilon\varepsilon_0 V_{TFL}/(ed^2) \quad (2)$$

where ε is the relative dielectric constant of $CsPbBr_3$ (≈22),[32] ε_0 is the vacuum permittivity, e is the electron charge, d is the distance between the Au electrodes (d ≈ 0.88 mm, Fig. S5, ESI†) and V_{TFL} is the trap-filled limit voltage (Fig. 4). Notably, the trap

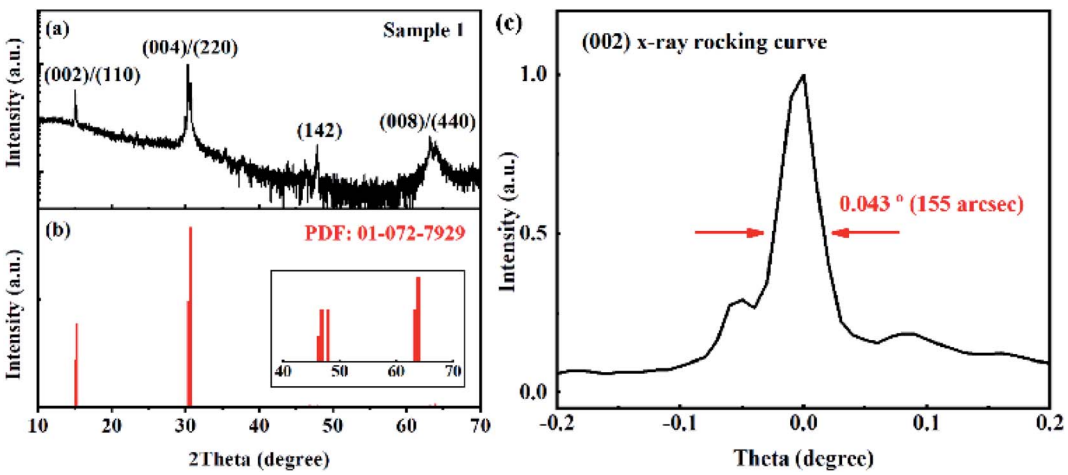

Fig. 2 Structural properties of as-grown $CsPbBr_3$ single crystal. Powder XRD patterns of (a) as-grown $CsPbBr_3$ single crystal and (b) $CsPbBr_3$ bulk material obtained from PDF card: 01-072-7929. (c) (002) XRC curve of as-grown $CsPbBr_3$ single crystal.

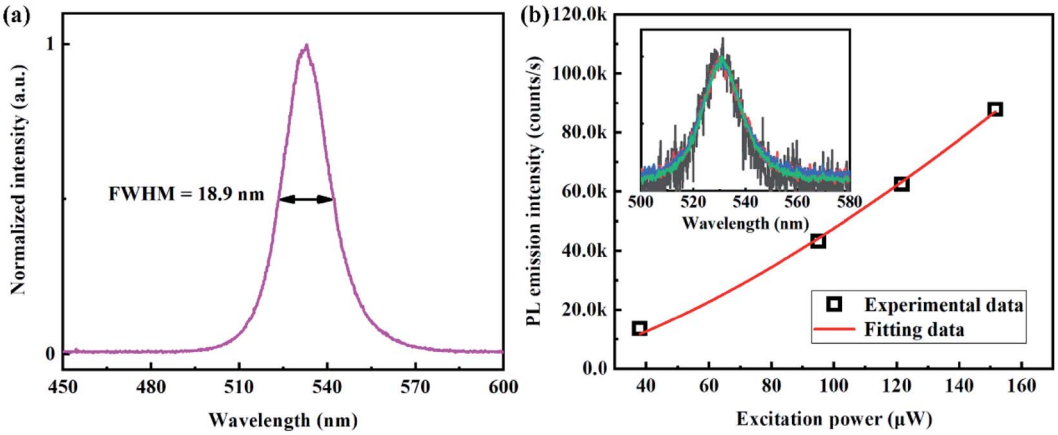

Fig. 3 Optical properties of as-grown $CsPbBr_3$ single crystal. (a) RT PL spectrum of as-grown $CsPbBr_3$ single crystal. (b) Excitation power dependence of PL emission intensities of as-grown $CsPbBr_3$ single crystal. The inset in (b) shows the normalized PL spectrum captured under different excitation power.

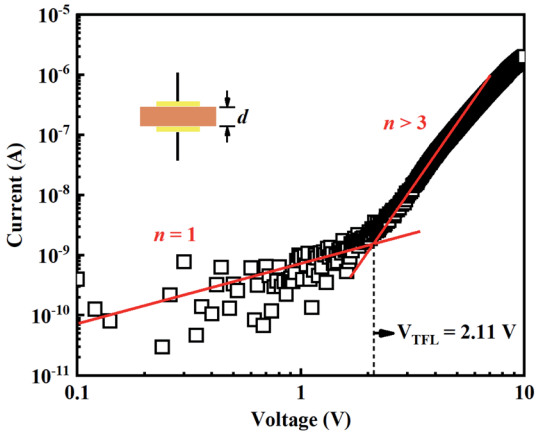

Fig. 4 I–V curve of an Au/$CsPbBr_3$/Au structured device. The I–V curve is fitted using a power law ($I \sim V^n$) (shown as red line).

density of our sample is about 1–2 orders of magnitude lower than similar perovskite single crystals reported in the literature (Table S1, ESI†) and about 7 orders of magnitude lower than spin-coated polycrystalline films.[33–35] Due to the low density of defects, the resistivity of as-grown $CsPbBr_3$ single crystal is as high as 1.8 GΩ, which is derived from the ohmic region of the I–V curve.

In the end, the mechanisms of crystal growth of $CsPbBr_3$ in the oil bath heating process are discussed. For the solution growth method (as shown in Fig. 1a), the growth kinetics of $CsPbBr_3$ is generally governed by the species transportation and diffusion at the solid/liquid interface. As a result, an uniform distribution of temperature field of precursor solution is prerequisite for growing high crystalline quality and low defects single crystals.[36] Here, the steady-state temperature field distribution of precursor solution shown in Fig. 1a was calculated using COMSOL Multiphysics packages, and the result is shown in Fig. 5a. It can be seen that the precursor solution is uniformly heated in the oil bath heating process. In this case, the crystal growth driving force is mainly related to constant and uniform supersaturation induced by the constant evaporation of solvent, which is responsible for the growth of high crystalline quality $CsPbBr_3$ single crystals with extremely low density of defects. On this basis, the growth process is proposed as follows: initially, the $CsPbBr_3$ nucleates when the precursor solution approaches saturation concentration (Fig. 5b). After that, a competitive $CsPbBr_3$ nucleus survives (labelled by blue box) and acts as a seed simultaneously, maintaining the subsequent crystal growth. In contrast, a temperature gradient was found when directly heating the precursor solution on the hot table (Fig. S6, ESI†). In this case, additional crystal growth driving forces related to the precursor concentration gradient

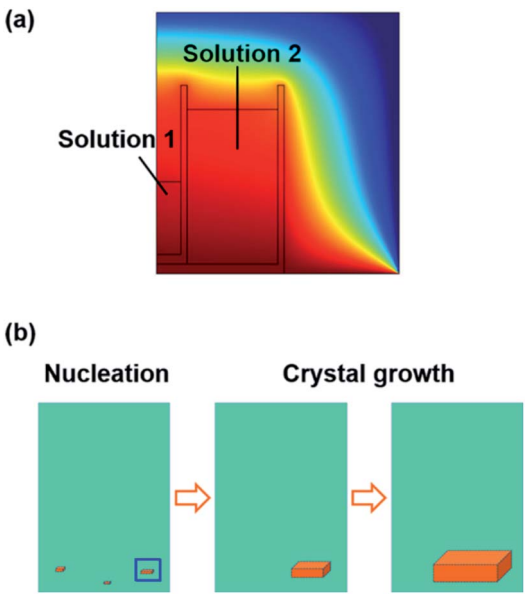

Fig. 5 (a) Calculated steady-state temperature field distribution of the precursor solution (labeled as solution 1) heated on the hot table with an oil bath (labeled as solution 2). (b) Proposed growth process of $CsPbBr_3$ single crystal.

can be expected, which accelerates the growth of $CsPbBr_3$ nucleus before they were re-dissolved. Meanwhile, the rapid growth rate will lead to a high defect density,[37] and further deteriorates the crystalline quality of the as-grown $CsPbBr_3$ single crystals.

Conclusions

In summary, we have shown a facile one-step solution growth method for growing high-quality all-inorganic $CsPbBr_3$ single crystals. By employing the oil bath heating strategy, the as-grown $CsPbBr_3$ single crystals have shown improved crystalline quality and extremely low density of defects, as verified by structural, optical, and electrical properties investigations. Simulation on the steady-state temperature field distribution indicated that the precursor solution was uniformly heated in the oil bath heating process, providing constant and uniform supersaturation as crystal growth driving force. This work provides a promising way to achieve high-quality all-inorganic $CsPbBr_3$ single crystals *via* a facile solution growth method.

Author contributions

Mingming Chen: conceptualization, methodology, writing – review & editing, funding acquisition. Chunxiang Xu: visualization, project administration. Youwen Yuan: investigation, writing – original draft. Yuan Liu: formal analysis, writing – review & editing. Dawei Cao: formal analysis, supervision, and writing – review & editing.

Conflicts of interest

There are no conflicts to declare.

Acknowledgements

This work was financially supported by the China Postdoctoral Science Foundation (2018M632196), and the Project of Faculty of Agricultural Equipment of Jiangsu University (NZXB20210202 and NZXB20200215).

Notes and references

1 G. Xing, N. Mathews, S. Sun, S. S. Lim, Y. M. Lam, M. Grätzel, S. Mhaisalkar and T. C. Sum, *Science*, 2013, **342**, 344.
2 G. Sathiyan, A. A. Syed, C. Chen, C. Wu, L. Tao, X. Ding, Y. Miao, G. Li, M. Cheng and L. Ding, *Nano Energy*, 2020, **72**, 104673.
3 C. Wu, C. Chen, L. Tao, X. Ding, M. Zheng, H. Li, G. Li, H. Lu and M. Cheng, *J. Energy Chem.*, 2020, **43**, 98–103.
4 X. Ding, C. Chen, L. Sun, H. Li, H. Chen, J. Su, H. Li, H. Li, L. Xu and M. Cheng, *J. Mater. Chem. A*, 2019, **7**, 9510–9516.
5 C. Chen, C. Wu, X. Ding, Y. Tian, M. Zheng, M. Cheng, H. Xu, Z. Jin and L. Ding, *Nano Energy*, 2020, **71**, 104604.
6 C. Chen, M. Cheng, H. Li, F. Qiao, P. Liu, H. Li, L. Kloo and L. Sun, *Mater. Today Energy*, 2018, **9**, 264–270.
7 **https://www.nrel.gov/pv/assets/pdfs/cell-pv-eff-emergingpv-rev211214.pdf**.
8 G. Xing, N. Mathews, S. S. Lim, N. Yantara, X. Liu, D. Sabba, M. Grätzel, S. Mhaisalkar and T. C. Sum, *Nat. Mater.*, 2014, **13**, 476–480.
9 F. Zhang, H. Zhong, C. Chen, X.-g. Wu, X. Hu, H. Huang, J. Han, B. Zou and Y. Dong, *ACS Nano*, 2015, **9**, 4533–4542.
10 Y. Wang, X. Li, J. Song, L. Xiao, H. Zeng and H. Sun, *Adv. Mater.*, 2015, **27**, 7101–7108.
11 J. Song, J. Li, X. Li, L. Xu, Y. Dong and H. Zeng, *Adv. Mater.*, 2015, **27**, 7162–7167.
12 M. Chen, Y. Yuan, Z. Wang, X. Shen, Y. Liu and D. Cao, *Cryst. Growth Des.*, 2020, **20**(8), 4855–4860.
13 X. Zheng, B. Chen, J. Dai, Y. Fang, Y. Bai, Y. Lin, H. Wei, X. C. Zeng and J. Huang, *Nat. Energy*, 2017, **2**, 17102.
14 X. Shen, M. Chen, L. Shi, F. Chen, Y. Liu, D. Cao and C. Xu, *Opt. Commun.*, 2019, **453**, 124354.
15 V. G. V. Dutt, S. Akhil and N. Mishra, *ChemNanoMat*, 2020, **6**, 1730–1742.
16 S. Akhil, V. G. V. Dutt and N. Mishra, *ChemNanoMat*, 2021, **7**, 342–353.
17 O. Nazarenko, S. Yakunin, V. Morad, I. Cherniukh and M. V. Kovalenko, *NPG Asia Mater.*, 2017, **9**, e373.
18 Y. Rakita, N. Kedem, S. Gupta, A. Sadhanala, V. Kalchenko, M. L. Böhm, M. Kulbak, R. H. Friend, D. Cahen and G. Hodes, *Cryst. Growth Des.*, 2016, **16**, 5717–5725.
19 M. I. Saidaminov, A. L. Abdelhady, G. Maculan and O. M. Bakr, *Chem. Commun.*, 2015, **51**, 17658–17661.
20 H. Zhang, X. Liu, J. Dong, H. Yu, C. Zhou, B. Zhang, Y. Xu and W. Jie, *Cryst. Growth Des.*, 2017, **17**, 6426–6431.
21 M. Zhang, Z. Zheng, Q. Fu, Z. Chen, J. He, S. Zhang, C. Chen and W. Luo, *J. Cryst. Growth*, 2018, **484**, 37–42.
22 M. I. Saidaminov, A. L. Abdelhady, B. Murali, E. Alarousu, V. M. Burlakov, W. Peng, I. Dursun, L. Wang, Y. He, G. Maculan, A. Goriely, T. Wu, O. F. Mohammed and O. M. Bakr, *Nat. Commun.*, 2015, **6**, 7586.
23 Y. Yuan, M. Chen, S. Yang, X. Shen, Y. Liu and D. Cao, *J. Lumin.*, 2020, **226**, 117471.
24 Z. Liu, Y. Bekenstein, X. Ye, S. C. Nguyen, J. Swabeck, D. Zhang, S.-T. Lee, P. Yang, W. Ma and A. P. Alivisatos, *J. Am. Chem. Soc.*, 2017, **139**, 5309–5312.
25 P. Acharyya, P. Pal, P. K. Samanta, A. Sarkar, S. K. Pati and K. Biswas, *Nanoscale*, 2019, **11**, 4001–4007.
26 X. Li, M. Chen, S. Mei, B. Wang, K. Wang, G. Xing and Z. Tang, *Sci. China Mater.*, 2020, **63**, 1510.
27 T. J. Whitcher, L. C. Gomes, D. Zhao, M. Bosman, X. Chi, Y. Wang, A. Carvalho, H. K. Hui, Q. Chang, M. B. H. Breese, A. H. Castro Neto, A. T. S. Wee, H. D. Sun, E. E. M. Chia and A. Rusydi, *NPG Asia Mater.*, 2019, **11**, 70.
28 K. Wei, Z. Xu, R. Chen, X. Zheng, X. Cheng and T. Jiang, *Opt. Lett.*, 2016, **41**, 3821–3824.
29 M. Zhang, Z. Zheng, Q. Fu, Z. Chen, J. He, S. Zhang, L. Yan, Y. Hu and W. Luo, *CrystEngComm*, 2017, **19**, 6797–6803.
30 D. Damberga, R. Viter, V. Fedorenko, I. Iatsunskyi, E. Coy, O. Graniel, S. Balme, P. Miele and M. Bechelany, *J. Phys. Chem. C*, 2020, **124**, 9434–9441.

31 J. Zeng, X. Li, Y. Wu, D. Yang, Z. Sun, Z. Song, H. Wang and H. Zeng, *Adv. Funct. Mater.*, 2018, **28**, 1804394.
32 M. I. Saidaminov, M. A. Haque, J. Almutlaq, S. Sarmah, X.-H. Miao, R. Begum, A. A. Zhumekenov, I. Dursun, N. Cho, B. Murali, O. F. Mohammed, T. Wu and O. M. Bakr, *Adv. Opt. Mater.*, 2017, **5**, 1600704.
33 A. R. Srimath Kandada, S. Neutzner, V. D'Innocenzo, F. Tassone, M. Gandini, Q. A. Akkerman, M. Prato, L. Manna, A. Petrozza and G. Lanzani, *J. Am. Chem. Soc.*, 2016, **138**, 13604–13611.
34 A. Solanki, S. S. Lim, S. Mhaisalkar and T. C. Sum, *ACS Appl. Mater. Interfaces*, 2019, **11**, 25474–25482.
35 H. Jin, E. Debroye, M. Keshavarz, I. G. Scheblykin, M. B. J. Roeffaers, J. Hofkens and J. A. Steele, *Mater. Horiz.*, 2020, **7**, 397–410.
36 K. Byrappa, in *Springer Handbook of Crystal Growth*, ed. G. Dhanaraj, K. Byrappa, V. Prasad and M. Dudley, Springer Berlin Heidelberg, Berlin, Heidelberg, 2010, pp. 599–653, DOI: **10.1007/978-3-540-74761-1_18**.
37 E. Huitema and J. P. van der Eerden, *J. Cryst. Growth*, 1996, **166**, 141–145.